Journal of
Nanoscience and Nanotechnology
Vol. 9, 7485–7490, 2009

Device Characteristics of Organic Light-Emitting Diodes Based on Electronic Structure of the Ba-Doped Alq_3 Layer

Jong Tae Lim, Kyung Nam Kim, and Geun Young Yeom*

School of Advanced Materials Science and Engineering, Sungkyunkwan University, Suwon 440-746, Korea

Organic light-emitting diodes (OLEDs) with a Ba-doped tris(8-quinolinolato)aluminum(III) (Alq_3) layer were fabricated to reduce the barrier height for electron injection and to improve the electron conductivity. In the OLED consisting of glass/ITO/4,4′,4″-tris[2-naphthylphenyl-1-phenylamino]triphenylamine (2-TNATA, 30 nm)/4,4′-bis[N-(1-napthyl)-N-phenyl-amino]-biphenyl (NPB, 18 nm)/Alq_3 (42 nm)/Ba-doped Alq_3 (20 nm, $x\% : x = 0$, 10, 25, and 50)/Al (100 nm), the device with the Alq_3 layer doped with 10% Ba showed the highest light out-coupling characteristic. However, as the Ba dopant concentration was increased from 25% to 50%, this device characteristic was largely reduced. The characteristics of these devices were interpreted on the basis of the chemical reaction between Ba and Alq_3 and the electron injection property by analyzing the electronic structure of the Ba-doped Alq_3 layer. At a low Ba doping of 10%, mainly the Alq_3 radical anion species was formed. In addition, the barrier height for electron injection in this layer was decreased to 0.6 eV, when compared to the pristine Alq_3 layer. At a high Ba doping of 50%, the Alq_3 molecules were severely decomposed. When the Ba dopant concentration was changed, the light-emitting characteristics of the devices were well coincided with the formation mechanism of Alq_3 radical anion and Alq_3 decomposition species.

Keywords: Organic Light-Emitting Diode, Electronic Structure, X-Ray Photoemission Spectroscopy, Ultraviolet Photoemission Spectroscopy, Near-Edge X-Ray Absorption Fine Structure.

1. INTRODUCTION

One of the critical issues for fabricating high-performance organic semiconductors such as organic light-emitting diodes (OLEDs), organic thin film transistors, organic solar cells, and organic sensors is to improve the property of carrier injection in the electrode/organic interface.[1–7] In OLEDs, the exciton recombination efficiency is limited by the number of injected electrons because most organic semiconductors are *p*-type and electron mobilities are in general lower than hole mobilities. Therefore, the efficient electron-injection is the key to improving the operation voltage and emission efficiency.[8] Recently, the OLED with a *p–i–n*-type structure, in which an intrinsic emission layer is embedded in between *n*- and *p*-type doped wide-gap organic electron and hole transport layers (ETL and HTL, respectively), have dramatically improved the device performance.[8] The OLEDs having electrically doped carrier-injecting/transporting layers exhibit low driving voltages with high carrier conductivity, which is due to the formation of radical anions, cations and ohmic contacts at the electrode interfaces.[9–12] Kido et al. demonstrated a device with a metal-doped ETL.[13] An *n*-type doped transporting layer was extended to developments of a Li-doped 4,7-diphenyl-1,10-phenanthroline (BPhen) layer, Li-doped Alq_3, and Li-doped 2,9-dimethyl-4,7-diphenyl-1,10-phenanthroline (BCP) layer by other researchers.[14–15] The high electrical conductivity of a Li-doped charge transporting layer is about 3×10^{-5} S/cm layer.[15]

In this *n*-doped carrier-transporting layer, the two important issues are the energy level alignment and the chemical reaction. The former is important in the aspect of electron injection, while the latter is essential for understanding the chemical process that leads to the degradation of the device. The electronic structure of the *n*-doped carrier-injecting layer plays an important role in determining their luminous efficiency and lifetime in the devices.

*Author to whom correspondence should be addressed.

 1533-4880/2009/9/7485/006 doi:10.1166/jnn.2009.1774

In this study, a new *n*-type carrier-transporting layer of Ba-doped Alq_3 was applied to OLEDs. The correlation between the device performance and the electronic features of a Ba-doped Alq_3 layer was investigated over a Ba doping range of 0 to 50%. In addition, the decomposition mechanism of the Alq_3 molecule composing the Ba-doped Alq_3 layer was studied as a function of Ba doping level.

2. EXPERIMENTAL DETAILS

The OLED was composed of glass/tin-doped indium oxide (ITO, about 10 Ω/□)/4,4′,4″-tris(2-naphthyl-phenyl-1-phenylamino)triphenylamine (2-TNATA, 30 nm)/4,4′-bis(N-(1-napthyl)-N-phenyl-amino)-biphenyl (NPB, 18 nm)/tris(8-quinolinolato)aluminium(III) (Alq_3, 42 nm)/Ba-doped Alq_3 (20 nm, *x*%)/Al (100 nm), with Ba doping levels of 0%, 10%, 25%, and 50% for devices 1–4, respectively. The emissive active area of all devices was 2×2 mm^2. All devices were vacuum-fabricated by thermal evaporation on glass/ITO substrates. In the fabrication of the Alq_3 layer doped with Ba at 10, 25, and 50%, the deposition rate for the Alq_3 matrix molecule was fixed at 0.2 nm/s while the deposition rates for the Ba dopant were varied as 0.02, 0.05, and 0.1 nm/s, respectively. Doping was achieved by co-evaporation, where the evaporation rates of Alq_3 and Ba were controlled independently by measuring with separate quartz thickness monitors. The current density–voltage–luminance characteristics were also measured using a Keithley 2400 electrometer, a photodiode (Oriel 71608), and a Keithley 485 picoammeter.

The electronic structure of the Ba-on-Alq_3 layer was examined by using X-ray photoemission spectroscopy (XPS), ultraviolet photoemission spectroscopy (UPS), and near-edge X-ray absorption fine structure (NEXAFS) spectroscopy at the 4B1 beam line in the Pohang Accelerator Laboratory (Korea). All the measurements and the deposition of the Ba-doped Alq_3 layer (10 nm) were performed in an ultra-high vacuum system, consisting of a main analysis chamber (approximately 5×10^{-10} Torr) and a sample preparation chamber (approximately 5×10^{-9} Torr). All samples were prepared *in-situ* by sequential thermal evaporation on a Si wafer, and all thicknesses were determined by timed depositions calibrated using a quartz-crystal microbalance. In the XPS studies, incident photon energies of 650 and 550 eV were used to obtain the core level spectra of O 1s and N 1s, respectively. For the UPS measurements, the He I (21.2 eV) line from a UV source was used. The photoemission onset reflecting the vacuum level at the surface of all samples was measured by biasing the samples at −20 V. The incident photon energy was calibrated by measuring the Au 4f level of a clean Au surface. In the NEXAFS analyses, N K-edge (387∼417 eV) and O K-edge (520∼560 eV) spectrum were measured at a photon incident angle of 45°.

3. RESULTS AND DISCUSSION

Figure 1(a) shows the current density–voltage–luminance characteristics for devices.[1–4] The device performance results are summarized in Table I. In Figure 1(a), the turn-on voltages (voltage at 0.1 cd/m^2, V_T) of devices 2–4 were 2.6, 2.6, and 2.8 V, respectively. However, the Ba-free device 1 showed the highest V_T value of 5.4 V. Meanwhile, at the luminance of about 100 cd/m^2 (V_{100}), the bias voltages of devices 2–4 were 4.0 (7.1), 4.6 (7.4), and 6.2 V (8.9 mA/cm^2), respectively, as seen in Figure 1(a). When the Alq_3 layer doped with 10% Ba was inserted between the cathode and Alq_3, the lowest power consumption (η_{PC}) was observed among the devices with a Ba-doped Alq_3 layer and the Ba-free device. Figure 2(b) shows the external quantum efficiency–current density–power efficiency characteristics for devices 2–4. At the luminance of 100 cd/m^2 (L_{100}), device 2 showed the highest device performance with an external quantum efficiency (η_{ext}) of 3.9 lm/W and a power efficiency (η_{PE}) of 2.0%. However, as the Ba dopant concentration was

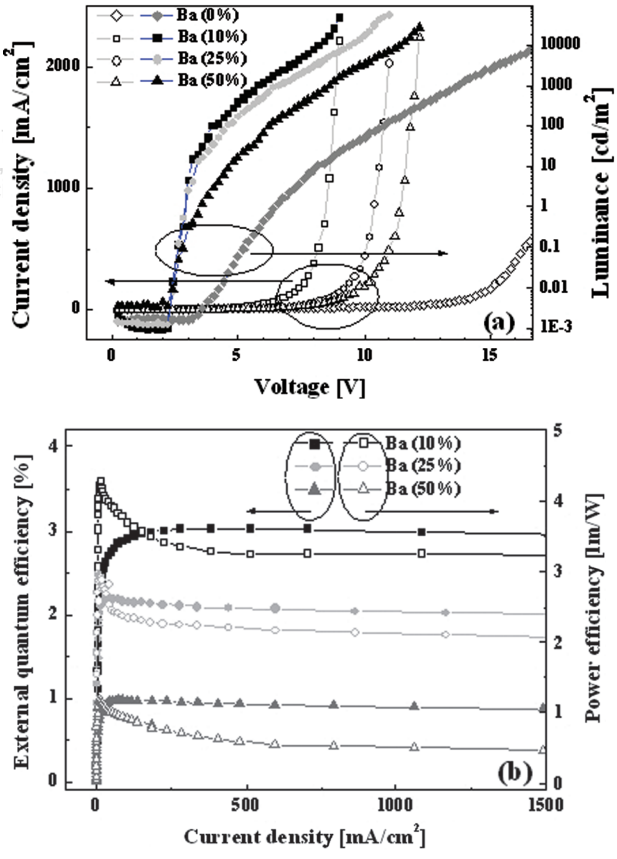

Fig. 1. (a) Current density–voltage–luminance and (b) external quantum efficiency–current density–power efficiency curves for devices 1–4. The devices were composed of glass/ITO/2-TNATA (30 nm)/NPB (18 nm)/Alq_3 (42 nm)/Ba-doped Alq_3 (20 nm, *x*%)/Al (100 nm). (*x*: the weight percentage concentration of Ba for devices 1–4 = 0 [diamond symbol], 10 [square symbol], 25 [circle symbol], and 50 [triangle symbol]).

Table I. Current density–voltage–luminance characteristics for devices 1–4.

Devices	Doping concentration of Ba (%)	η_{ext} (%)	η_{PE} (lm/W)	V_{100} (V)	V_T (V)	L_{max} (cd/m^2)
1	0	—	—	—	5.2	—
2	10	2.0	3.9	4.0 (7.1 mA/cm^2)	2.6	47850 at 9.0 V
3	25	1.5	2.6	4.6 (7.3 mA/cm^2)	2.6	43140 at 10.6 V
4	50	0.7	1.2	6.2 (8.9 mA/cm^2)	2.8	28350 at 12.2 V

η_{ext}, η_{PE}, and V_{100} are the values at 100 cd/m^2. V_T and L_{max} are the turn-on voltage at a luminance of 0.1 cd/m^2 and the maximum luminance, respectively.

increased from 10 to 50%, η_{ext} and η_{PE} were abruptly reduced. The results of η_{PC}, η_{ext}, and η_{PE} demonstrated the dependence of the device performance on the characteristics of the Ba-doped Alq_3 layer. The device performance was maximized with the 10% Ba-doped Alq_3 layer, but was deteriorated with further increase in the Ba doping. To elucidate the mechanism involved in the enhancement of the device performance, the electronic structures of the Ba-doped Alq_3 layer were investigated as a function of Ba dopant concentration.

Figure 2(a) shows the evolution of the O 1s electron density curves (EDCs) as a function of the weight percentage of Ba in the Ba-doped Alq_3 layer, as measured by XPS. For the pristine Alq_3 layer, the O 1s core-level EDC was symmetrical in shape and was composed of a single component, indicating a clean Alq_3 film. The single component of the O 1s EDC was initially shifted to a higher binding energy of 532.2 eV (Alq_3 radical anion formed by electron charge transfer (ECT) from Ba) until the Ba dopant concentration of 10%, compared with pristine Alq_3 of 531.6 eV. From the Ba dopant concentration of 25%, the O 1s peak of 530.6 eV (decomposition by Al–O bond breaking) began to appear with low intensity at a lower binding energy, and the intensity of the 530.6 eV

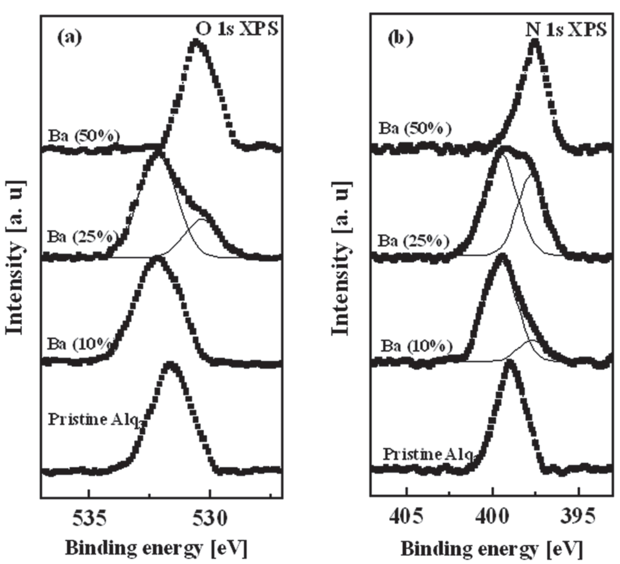

Fig. 2. The evolution of XPS O 1s (a) and N 1s (b) core level EDCs as a function of the weight percentage of Ba in the Ba-doped Alq_3 layer. The values in the figures indicate the weight percentage of Ba.

peak was further increased at the dopant concentration of 50%. The peak shift to a lower binding energy was caused by a decrease in the Coulomb potential between the nuclei and the electrons of the O 1s core level as a result of the increased electron density at the valence band of O atoms due to an electron provided by Ba.[2]

Meanwhile, Choong et al. reported that the binding energy difference between an Alq_3 radical component and a decomposition component in the Ca/Alq_3 interface was 2.0 eV in the XPS spectra of O 1s.[16] The large peak shift of 1.6 eV between the Alq_3 radical species and Alq_3 decomposition species, as shown in Figure 2(a), indicates bond breakage between the Al and O atoms in the Alq_3 molecule. Therefore, the peak at a low binding energy of 530.6 eV was attributed to the appearance of a metallic Alq_3 component that was decomposed by the large ECT from Ba at the higher Ba concentration. Figure 2(b) shows the N 1s core level EDCs as a function of the Ba dopant concentration ranging from 0 to 50%. Even with the lowest Ba dopant concentration of 10%, Alq_3 decomposition species (around 397.6 eV) reacting with Ba was observed with Alq_3 radical species (around 399.5 eV). This indicates that Ba interacts with N before O, which is reasonable given that the Al–N bond is the weakest as the coordinated bonding[17] in the Alq_3 molecule. Considering the dependence of the device characteristics shown in Figure 1 on the Ba dopant concentration, the formation of the decomposition component in the N XPS spectra did not affect the decomposition of Alq_3 molecules at any of the Ba dopant concentrations. However, the emergence of the decomposition component leading to the breakage of the Al–O ionic bonding[17] in the O XPS spectra provides a direct cause of the poor device performance at the Ba dopant concentration of above 10%.

Figure 3(a) shows the NEXAFS spectra at the N K-edge of the Ba-doped Alq_3 layer over the Ba dopant concentration range of 0 to 50%. NEXAFS spectroscopy shows the resonance features induced by a transition from the initial state (core level) to the final state (vacant level), and can be used to obtain information on the unoccupied state. Curioni et al.[18] reported peaks at 392.9, 400.5, and about 403.0 eV in pristine Alq_3 due to the transitions of electrons from the N 1s level to the lowest unoccupied molecular orbital (LUMO), LUMO + 2 (and LUMO + 3), and many σ^*, respectively. The spectrum from pristine Alq_3 was in

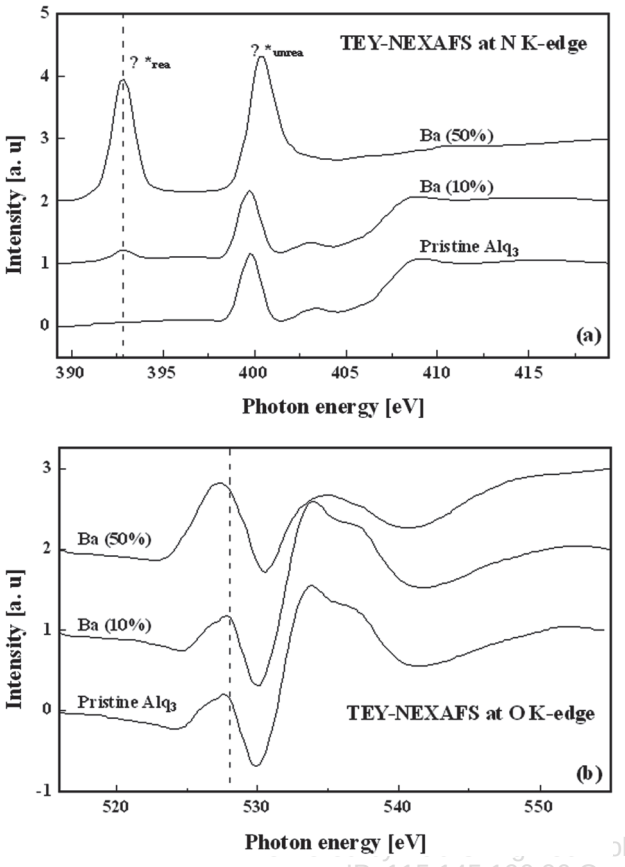

Fig. 3. Total electron yield (TEY) near-edge X-ray absorption fine structure (NEXAFS) spectra at the N K-edge (a) and O K-edge (b) of the Ba-doped Alq_3 layer over a weight percentage concentration of Ba from 0 to 50%. The π^*rea and π^*unrea indicate the transitions, from N core level to π^* levels, of nitrogen species reactive with Ba and those unreactive with Ba, respectively.

good agreement with the results of Curioni et al.[18] Interestingly, new resonance peaks appeared at 392.9 eV upon Ba adsorption.

The peaks at 392.9 and 400.5 eV, which were induced by the transition to LUMO levels consisting of π^* unoccupied states, were attributed to π^*rec (species of N atom reacted with Ba) and π^*unrec (species of N atom unreacted with Ba), respectively. The difference (7.6 eV) in the large photon energy between π^*rec and π^*unrec was interpreted as being caused by the change in the final state, because the N 1s core level does not show any strong feature related with the chemical modification, as shown in Figure 2(b). The appearance of a π^*rec peak even at the Ba concentration of 10% on Alq_3 indicated that the orbitals involved with ECT were mainly localized at the pyridyl ring[17] rather than the phenoxide ring[17] on the 8-quinolinolato ligand composing the Alq_3 molecule. Furthermore, no π^*rec peak appeared in the interfaces of K/Alq_3 [19] and Cs/Alq_3 [20] in the NEXAFS spectra. These results indicated that electron charge injection could be more improved by Ba than by K (or Cs) because Ba could provide more electrons than K (or Cs) to the orbitals involved with the pyridyl ring composing the Alq_3 molecules. Therefore, Alq_3 incorporating Ba is expected to show superior device performance than K (or Cs). Meanwhile, the ratio of π^*rec/π^*unrec in Figure 3(a) was increased with increasing Ba dopant concentration. This result was in agreement with the increasing tendency of the π^*rec/π^*unrec ratio with increasing Ba dopant concentration, as shown in Figure 2(b).

Figure 3(b) shows the NEXAFS spectra at the O K-edge of the Ba-doped Alq_3 layer over the Ba dopant concentration range of 0 to 50%. The peaks at 528 and 534 eV in pristine Alq_3 were due to the transitions of electrons from the O 1s level to LUMO (and LUMO+2) and many σ^*, respectively.[18] As shown in the NEXAFS spectra of Figures 3(a and b), the shape of each atom-resolved electronic spectrum that is mainly composed of Alq_3 radical anion species (10% doping) was very similar to that of the pristine Alq_3 (0% doping). However, the transition of the Alq_3 decomposition species (50% doping) showed a large difference to that of pristine Alq_3 (0% doping), due to the destroyed Alq_3 molecular structure.

Figure 4(a) shows the UPS spectra around the highest occupied molecular orbitals (HOMOs) of the pristine Alq_3 layer and the Alq_3 layer doped with 10% Ba. The HOMO level in the Alq_3 layer doped with 10% Ba was shifted to a binding energy 0.6 eV higher than that of the pristine Alq_3 layer. This lowering of the HOMO level implied that the barrier height for electron injection was lowered.[2] In addition, as shown in Figure 4(a), the metal-induced gap state (MIGS),[21] which is roughly a free-electron-like, metal wave function penetrating into the organic semiconductor side, was observed at the forbidden energy gap of approximately 1.6 eV above the HOMO of Alq_3. The band of the Ba-doped Alq_3 layer was realigned due to the introduced MIGS and work function (WF) difference.[22] In fact, a new gap state has also been observed in several interfaces between a low WF metal (e.g., Li, Na, K, Ca, and Mg) and Alq_3.[23] The inset of Figure 4(a) shows the photoemission onset measured at the pristine Alq_3 layer and the Alq_3 layer doped with 10% Ba, with a sample bias of −20 V, reflecting the WF shifts of Alq_3 achieved by Ba adsorption.

Figure 4(b) shows the proposed energy band diagram for the pristine Alq_3 layer and the Alq_3 layer doped with 10% Ba. The WF ($\Delta\Phi = \Phi Alq_3 - \Phi$Ba-doped Alq_3) and HOMO level (ΔHOMO = HOMOAlq_3 − HOMOBa-doped Alq_3) shifts were obtained from Figures 4(a) and (b) respectively. The energy band gap (E_g) of pristine Alq_3 was 2.9 eV.[2] The Alq_3 layer doped with 10% Ba showed a low barrier height for an electron injection of 0.2 eV due to the lowering of the HOMO level. This lowering of 0.6 eV in the HOMO level in the Alq_3 layer doped with 10% Ba was due not only to band bending by Fermi level pinning, but also to the chemical modification of the Alq_3 molecules by the excess electrons of the Ba metal.

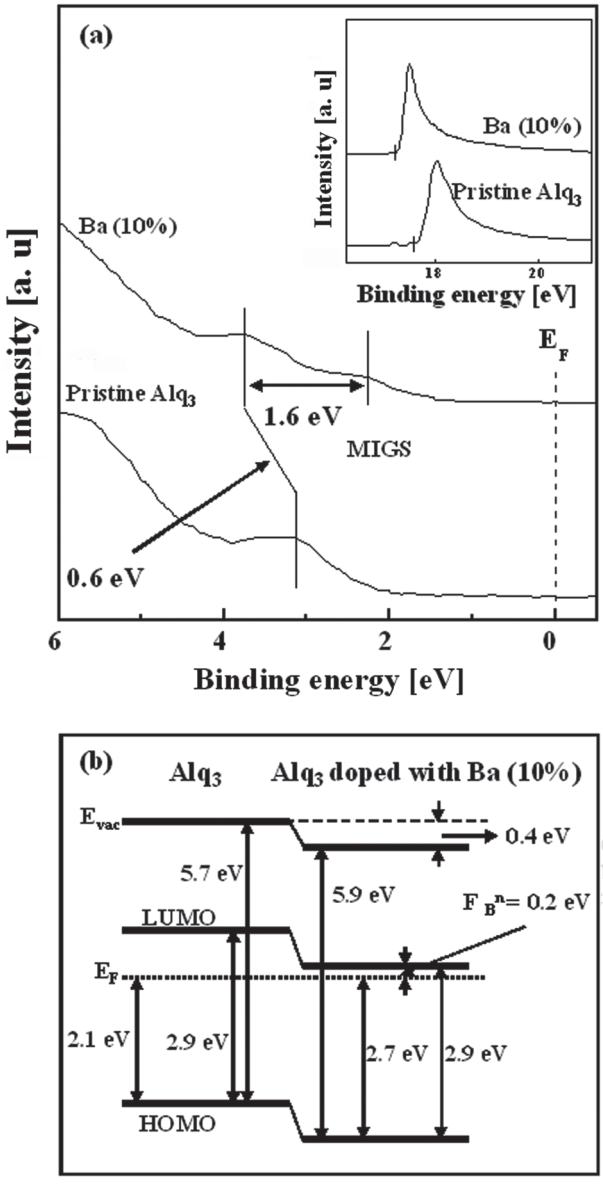

Fig. 4. (a) Ultraviolet photoemission spectrum (UPS) around the HOMO of the pristine Alq_3 layer and the Alq_3 layer doped with 10% Ba. The inset shows the onset of photoemission, indicating the vacuum level of the Ba-doped Alq_3 layer. (B) Proposed energy band diagram for the pristine Alq_3 layer and the Alq_3 layer doped with 10% Ba.

Moreover, the presence of MIGS in the Ba-doped Alq_3 layer, as shown in Figure 4(a), is further evidence for the chemical reaction between Ba and Alq_3.

4. CONCLUSIONS

In conclusion, we investigated the mechanism of the improved device performance achieved by inserting the Ba-doped Alq_3 layer between the cathode and the ETL. The performance of the device comprising the Alq_3 layer doped with 10% Ba was enhanced by the reduction of the HOMO level by 0.6 eV, as shown in the UPS spectra. This reduction was due to the MIGS formed by chemical reaction as well as the band bending formed by Fermi level pinning. Although the electron-injecting barrier height of the Ba-doped Alq_3 at all dopant concentrations used in this study was almost identical, the interface chemistry largely depended on the Ba dopant concentration, as shown in the reactive species in the XPS spectra (O 1s and N 1s), and the NEXAFS spectra at the N and O K-edge. The formation of stable Alq_3 radical anion species at the low Ba concentration of 10% enhanced the OLED device performance but the appearance of Alq_3 decomposition species from the Ba concentration of 25% degraded the device performance due to Al–O, rather than Al–N, bond breaking in the Ba-doped Alq_3 layer.

Acknowledgment: This research was supported by a grant (PAD-4) from the Information Display R&D Center, one of the 21st Century Frontier R&D Programs funded by the Ministry of Knowledge Economy of the Korean government. This work were also supported by Pohang Accelerator Laboratory in Korea and by the WCU program of Korea Science and Engineering Foundation funded by the Korean government (MOEHRD) (Grant No. R32-2008-000-10124-0).

References and Notes

1. L. L. Chua, J. Zaumseil, J.-F. Chang, E. C. W. Ou, P. K. H. Ho, H. Stirringhaus, and R. H. Friend, *Nature* 434, 194 (**2005**).
2. H. Ishii, K. Sugiyama, E. Ito, and K. Seki, *Adv. Mater.* 11, 605 (**1999**).
3. K. Y. Wu, Y. T. Tao, and H. W. Huang, *Appl. Phys. Lett.* 99, 241104 (**2007**).
4. C. W. Tang, *Appl. Phys. Lett.* 48, 183 (**1986**).
5. L. Wang, D. Fine, D. Sharma, L. Torsi, and A. Dodabalapur, *Anal. Bioanal. Chem.* 384, 310 (**2006**).
6. J. H. Lee, H. Y. Chu, J. I. Lee, K. I. Song, and S. J. Lee, *J. Nanosci. Nanotechnol.* 8, 5185 (**2008**).
7. B. C. Kwack, K. S. Lee, D. C. Choo, T. W. Kim, J. H. Seo, and Y. K. Kim, *J. Nanosci. Nanotechnol.* 8, 5532 (**2008**).
8. L. C. Palilis, M. Uchida, and Z. H. Kafafi, *IEEE J. Sel. Top. Quantum Electron* 10, 1 (**2004**).
9. J. S. Huang, M. Pfeiffer, A. Werner, J. Blochwitz, K. Leo, and S. Y. Liu, *Appl. Phys. Lett.* 80, 139 (**2002**).
10. J. M. Bharathan and Y. Yang, *J. Appl. Phys.* 84, 3207 (**1998**).
11. A. Yamamori, C. Adachi, T. Koyama, and Y. Taniguchi, *Appl. Phys. Lett.* 72, 2147 (**1998**).
12. X. Zhou, J. Blochwitz, M. Pfeiffer, A. Nollau, T. Fritz, and K. Leo, *Adv. Funct. Mater.* 11, 310 (**2001**).
13. J. Kido and T. Matsumoto, *Appl. Phys. Lett.* 73, 2866 (**1998**).
14. J. Huang, M. Pfeiffer, A. Werner, J. Blochwitz, K. Leo, and S. Liu, *Appl. Phys. Lett.* 80, 139 (**2002**).
15. G. Parthasarathy, C. Shen, A. Kahn, and S. R. Forrest, *J. Appl. Phys.* 89, 4986 (**2001**).
16. V. E. Choong, M. E. Mason, C. W. Tang, and Y. Gao, *Appl. Phys. Lett.* 72, 2689 (**1998**).
17. C. H. Chen and J. Shi, *Coordi. Chem. Rev.* 171, 161 (**1998**).
18. A. Curioni, W. Andreoni, R. Treusch, F. J. Hinpsel, E. Haskal,

P. Seidler, C. Heske, S. Kakar, T. van Buuren, and L. J. Terminello, *Appl. Phys. Lett.* 72, 1575 **(1998)**.
19. T. Yokoyama, H. Ishii, N. Matsuie, K. Kanai, E. Ito, A. Fujimori, T. Araki, Y. Ouchi, and K. Seki, *Synth. Metals* 152, 277 **(2005)**.
20. J. T. Lim, J. H. Lee, Y. S. Kim, and G. Y. Yeom, *J. Korean Phys. Soc.* 52, 476 **(2008)**.
21. M. Kiguchi, R. Arita, G. Yoshikawa, Y. Tanida, S. Ikeda, S. Entani, I. Nakai, H. Kondoh, K. Saiki, and H. Aoki, *Phys. Rev.* 72, 75446 **(2005)**.
22. J. Tersoff, *Phys. Rev. Lett.* 52, 465 **(1984)**.
23. C. Shen, I. G. Hill, A. Kahn, and I. Schwartz, *J. Am. Chem. Soc.* 122, 5391 **(2000)**.

Received: 9 October 2008. Accepted: 17 March 2009.